Study on the structural and electromagnetic properties of Tm-substituted Mg–Mn ferrites by a solution combustion method

Nilar Lwin [a,*], Radzali Othman [b], Srimala Sreekantan [c], M.N. Ahmad Fauzi [c,*]

[a] Department of Mechanical Engineering, University of Malaya, 50603 Kuala Lumpur, Malaysia
[b] Faculty of Manufacturing Engineering, Universiti Teknikal Malaysia Melaka, 76100 Durian Tunggal, Malacca, Malaysia
[c] School of Materials and Mineral Resources Engineering, Universiti Sains Malaysia, Engineering Campus, 14300 Nibong Tebal, Penang, Malaysia

ARTICLE INFO

Article history:
Received 7 August 2014
Received in revised form
12 March 2015
Accepted 12 March 2015
Available online 13 March 2015

Keywords:
Spinel ferrite
Solution combustion
Microstructure
Tm substitution
Magnetic property
Electrical property

ABSTRACT

The effect of thulium ion substitution for iron on the structural and electromagnetic properties of Mg–Mn ferrites is reported. The $Mg_{0.9}Mn_{0.1}Tm_xFe_{1.8-x}O_4$ ferrite compositions with $x=0.0$, 0.025, 0.05, and 0.075 were synthesized by a nitrate–citrate solution combustion method. Tm substitution had taken place and this was found to produce a secondary phase $TmFeO_3$. The crystallite size of the powder calcined at 500 °C was in the range of 9–13 nm. Subsequently, the calcined ferrite powders were compacted and sintered at 1250 °C. It was found that the physical and magnetic properties had changed with Tm contents. Bulk density was found to decrease from 4.26 to 3.82 g/cm^3 with increasing Tm contents. It was also found that the saturation magnetization ($M_s=38.41$–23.62 emu/g) had decreased with an increase of Tm. In this study, the highest resistivity ($39.84\times10^6\ \Omega$ cm) was observed for $Mg_{0.9}Mn_{0.1}Fe_{1.725}Tm_{0.075}O_4$. The correlation between structural and electromagnetic properties of the Tm-substituted samples is interpreted based on phase composition as well as microstructure.

1. Introduction

Magnetic spinel ferrites are important materials due to their excellent electrical and magnetic properties, viz. low dielectric constant, low dielectric losses, high resistivity, low coercivity and low saturation magnetization [1]. With these outstanding properties, they are used in the fabrication of magnetic, electronic and microwave devices. The electrical and magnetic properties of ferrites had been reported to be strongly dependent on the purity of the starting ferrite powder, the microstructure as well as the grain boundary chemistry [2]. Typically, high purity, uniform composition and good microstructure developed are essential for the high performance of the ferrites [3]. Improved electromagnetic properties of ferrites are crucial for the miniaturization of components in electronic devices. They are widely used in high frequency applications since an AC field does not induce undesirable eddy currents in an insulating material [4].

Various synthesis methods have been accordingly developed to produce ferrite particles including citrate precursor, hydrothermal, co-precipitation, solution combustion methods, etc. [5–7]. Among these methods, the solution combustion method is an effective method to achieve high purity with excellent compositional control and crystalline nano-ferrite powders. Typically, the reactions during a combustion method can be influenced by a number of parameters, including the type of fuel, the fuel-to-oxidizer ratio (*f*/*o*), the water content of the precursor mixture and the ignition temperature [8,9]. Glycine, urea and citric acid are some of the commonly used fuels for combustion [10]. Among the organic complexants, citric acid has a good capability of providing chelating metallic ions with low decomposition temperatures (175 °C) and the least heat of combustion (10.2 kJ/g) [11]. Based on these reviews of pertinent past research works, citric acid was chosen, in this research work, as the fuel to obtain precursors of transition metal oxides.

Recently, ferrites substituted with rare-earth elements have been found to be promising materials to be used for different applications in modern device technology. An addition of small amounts of rare-earth cations to ferrite samples not only changes the structural properties but also their electromagnetic properties, depending upon the type and amount of the rare-earth element used [12].

Numerous related studies had been conducted on the influence of different rare-earth atoms (La, Ce, Pr, Nd, Pm, Sm, Sc, Eu, Gd, Tb, Dy, Ho, Er, Tm, Yb, and Lu) on the properties of ferrites [13–15]. As a consequence of these works, it was established that different rare-earth atoms have different effects on spinel ferrites. To date, there is no investigation reporting on the effect of Tm

* Corresponding authors.
E-mail addresses: nilarlwin@um.edu.my (N. Lwin), srafauzi@usm.my (M.N. Ahmad Fauzi).

http://dx.doi.org/10.1016/j.jmmm.2015.03.046
0304-8853/

substitutions on the properties of Mg–Mn ferrites. Therefore, in the present work, the effect of Tm^{3+} substitution for Fe^{3+} on the structural and electromagnetic properties of Mg–Mn ferrites will be described.

2. Experimental

Mg–Mg ferrites substituted with rare-earth ions Tm were prepared using a solution combustion method. The chemical reagents for this experiment were $Fe(NO_3)_2 \cdot 9H_2O$ (Aldrich, 99.8%), $Mg(NO_3)_2 \cdot 6H_2O$ (Sigma-Aldrich 99%), $Mn(NO_3)_2 \cdot 6H_2O$, $Tm(NO_3)_2 \cdot 6H_2O$ and citric acid (Sigma-Aldrich 99.5%). Firstly, the metal nitrates and citric acid were dissolved in deionized water with a 1:1 M ratio of metal to citric acid. Each mixture prepared was ensured to be of 10 g per batch. The mixture of solutions was heated on a hotplate set at 80 °C. Upon the formation of a dense sticky gel, the temperature was increased to 120 °C for the dehydrating process. The temperature was then increased rapidly and when it reached to ~200 °C, large amount of gases (CO_2, H_2O, N_2) were liberated and a dark brown ferrite mass was produced through the combustion process. The as-burnt mass was heated (commonly referred to as calcined) in air at 500 °C for 5 h. The calcined mass was then ground manually using an agate pestle and mortar. The resultant powder was subsequently pressed uniaxially in a 13 mm diameter stainless steel die at a pressure of 100 MPa to form a disk. The disk specimens obtained were finally sintered at 1250 °C in air. Diffractograms were recorded using an X-ray diffractometer (Bruker Advanced D8), operated at 40 kV and 20 mA. A CuKα radiation source was used to determine whether a single-phase cubic spinel structure was formed in the as-burnt powders, calcined powders, as well as the sintered specimens. A transmission electron microscope (Philips CM 12) was used for structural characterization of the calcined ferrite powders. Bulk density and apparent porosity of sintered specimens were determined using the Archimedes principle. The magnetic properties were measured using vibrating sample magnetometer (VSM) (model-7410, Lake Shore). The dielectric properties such as resistivity, dielectric constant and dielectric loss of the sintered pellets were measured using an impedance analyser (HP/Agilent 4291B RF).

3. Results and discussion

3.1. X ray analysis

Fig. 1 shows the XRD diffractograms of the as-burnt Tm-substituted Mg–Mn ferrite powders. The phase analysis indicates that the as-burnt ferrite powders are partially crystalline (ICDD number 01-0881938) in nature and contain a spinel ferrite phase. The broad peaks of the diffractograms are indicative of the fine crystallite size in the ferrite [16].

The crystallite size was calculated using the Scherrer formula [17]. The crystallite size of the various Tm-substituted as-burnt powders was found to be in the range of 5–10 nm. The crystallinity of the homogeneous spinel phase in the as-burnt powders, calcined at 500 °C for 5 h, also shows an increase as indicated in Fig. 2. The crystallite size of the calcined powder is found to be in the range of 9–13 nm. It is observed that the broadening of the diffraction peaks decrease upon comparing the as-burnt to the calcined powders. Inherently, the crystallite size increases with successive heat-treatment of the ferrite.

The ferrites sintered at 1250 °C were also characterized by XRD. Fig. 3 shows the diffractograms of the various sintered ferrites. All the Tm ferrite compositions indicate the presence of a spinel Mg–Mn ferrite as the major phase. Tm-substituted specimens (Fig. 3b–d) also show the presence of a $TmFeO_3$ phase [ICDD 00-046-0114]

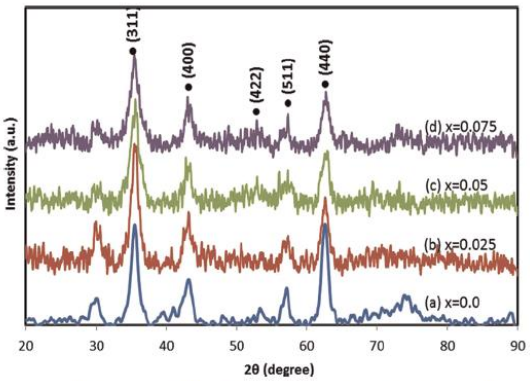

Fig. 1. XRD diffractograms of $Mg_{0.9}Mn_{0.1}Fe_{2-x}Tm_xO_4$ ferrite of as-burnt powder. (a) $x=0.0$, (b) $x=0.025$, (c) $x=0.050$, and (d) $x=0.075$.

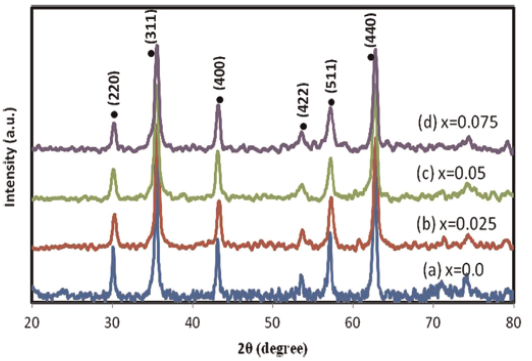

Fig. 2. XRD diffractograms of $Mg_{0.9}Mn_{0.1}Fe_{2-x}Tm_xO_4$ ferrite powder calcined at 500 °C for (a) $x=0.0$, (b) $x=0.025$, (c) $x=0.050$, and (d) $x=0.075$.

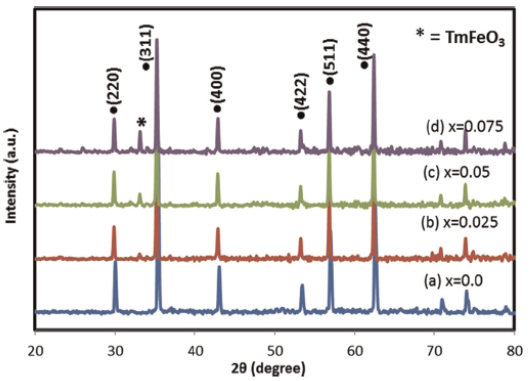

Fig. 3. XRD diffractograms of $Mg_{0.9}Mn_{0.1}Fe_{2-x}Tm_xO_4$ ferrites sintered at 1250 °C for (a) $x=0.0$, (b) $x=0.025$, (c) $x=0.05$, and (d) $x=0.075$.

together with the dominant Mg–Mn ferrite phase. The intensity of $TmFeO_3$ increases with an increase of Tm contents. This apparently indicates that Tm does not form a solid solution with the spinel ferrite or Tm^{3+} has limited solid solubility [18]. When the solubility limit is attained, no further Tm is diffused into the spinel lattice. Subsequently, Tm ions accumulate at the grain boundaries

and combine with Fe to produce $TmFeO_3$. Hence, a thin insulating layer is formed around the grains [19]. The $TmFeO_3$ formed can be observed in the microstructural results (Fig. 7).

In order to highlight the appearance of the second phase ($TmFeO_3$) in substituted ferrites, the XRD analysis was conducted on samples after the different stages of processing and firing. Fig. 4 shows the XRD diffractograms of the as-burnt, calcined and sintered ferrites for $x=0.025$ composition. The secondary phase, $TmFeO_3$, is not detected in all of the as-burnt and calcined powders for the various compositions. However, the $TmFeO_3$ phase is detected in all sintered samples (1250 °C).

The absence of $TmFeO_3$ in the as-burnt and calcined powders

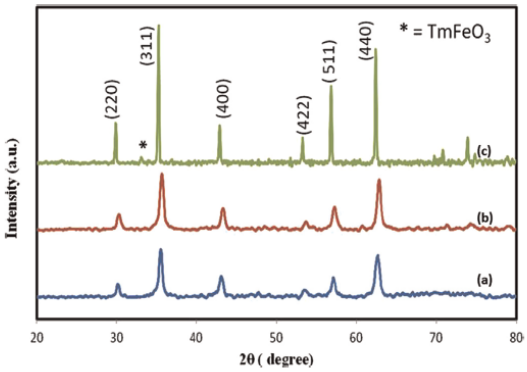

Fig. 4. XRD diffractograms of $Mg_{0.9}Mn_{0.1}Fe_{1.8-x}Tm_xO_4$ ferrites with $x=0.025$ in (a) as-burnt powder, (b) calcined powder and (c) sintered samples.

may be due to the formation of a non-crystalline product or an amorphous phase due to the very rapid rate of reactions upon combustion. Upon increasing the duration of heat treatment (up to the sintering stage), the crystallinity of this second phase increases in sintered specimens that can be clearly observed in Fig. 4. A similar trend of increasing crystallinity of a second phase with sintering was observed in rare-earth (La substituted) Mg–Cd ferrites as reported by Gadkari et al. [20]. They found that a $LaFeO_3$ phase was detected in all their sintered specimens.

The presence of a secondary phase indicates that the substituents have a solubility limit in the spinel lattice. It is known that the degree of replacement of the Fe^{3+} ions by other ions in the spinel lattice depends on the radius of the substituent cation. Since the ionic radius of Tm^{3+} (0.102 nm) is larger than that of Fe^{3+} (0.064 nm), the replacement of Fe^{3+} by Tm^{3+} is limited in the spinel lattice.

3.2. TEM microstructural analysis

Figs. 5 and 6 show the TEM images of the particles and particle size distributions (histogram) of Tm-doped Mg–Mn ferrites, respectively. The images show that the particles obtained by this synthesis method are uniform in morphology as well as particle size, but clearly agglomerated to some extent. The average particle size of the samples for all the compositions calculated using an Image J software is in the range of ~8–13 nm. It is observed from the images that the particles sizes of the Tm-doped samples are smaller than that of the undoped samples. This behavior is similar to that of Sm-doped NiCuCr ferrites as reported by Yanmin et al. [21]. It is expected that the smaller particle size could grow into smaller grains in sintered specimens. Generally, the smaller grains imply a larger number of insulating grain boundaries which act as

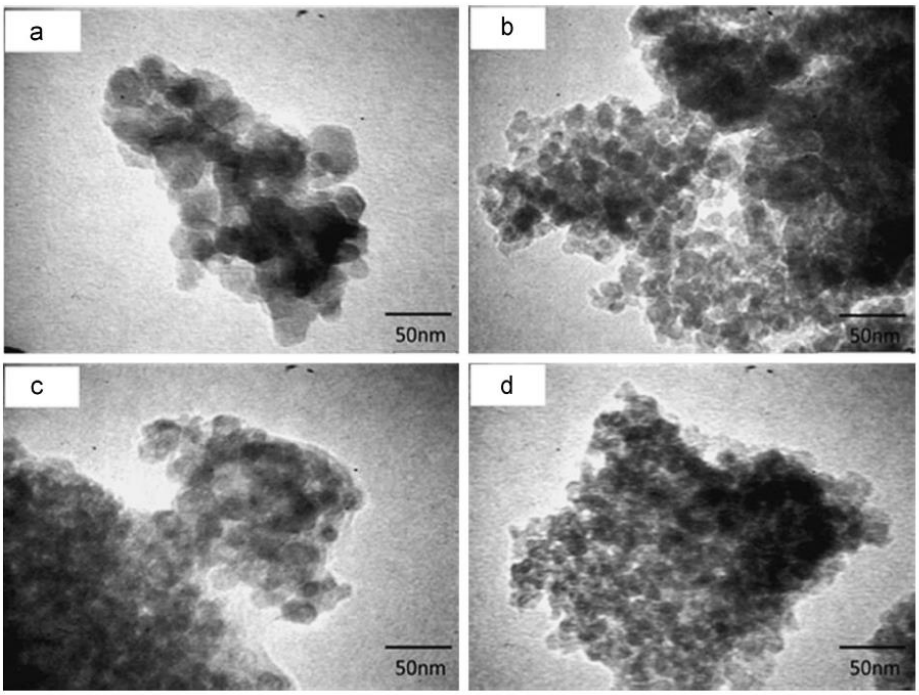

Fig. 5. TEM images of $Mg_{0.9}Mn_{0.1}Tm_xFe_{1.8-x}O_4$ ferrite particles. (a) $x=0.0$, (b) $x=0.025$, (c) $x=0.050$ and (d) $x=0.075$.

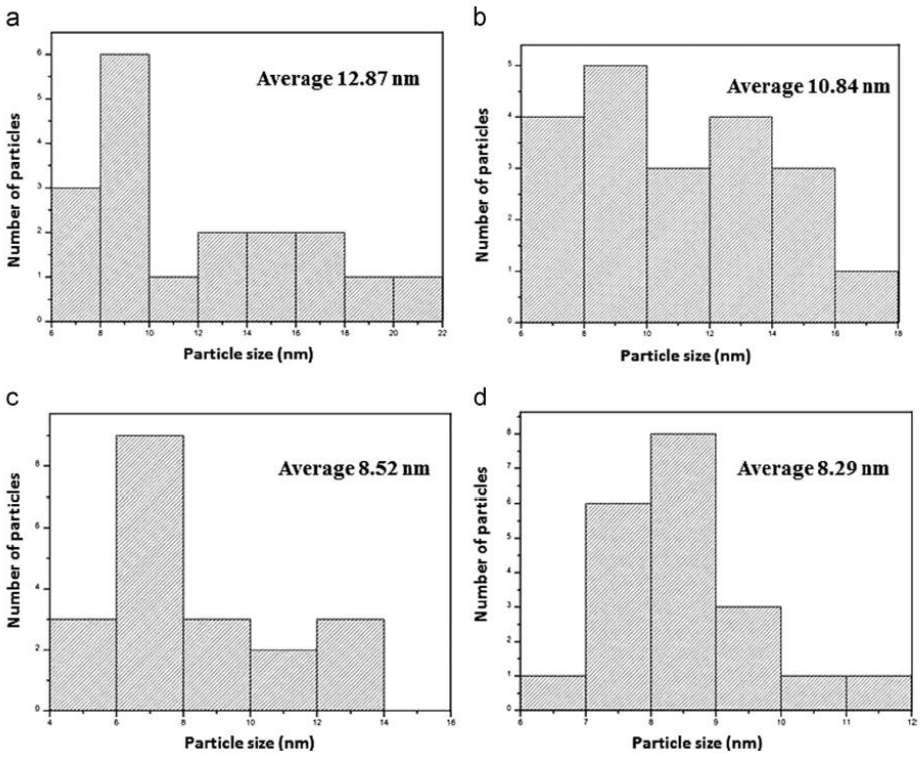

Fig. 6. Particle size distribution histograms of $Mg_{0.9}Mn_{0.1}Tm_xFe_{1.8-x}O_4$ ferrite nanoparticles. (a) $x=0.0$, (b) $x=0.025$, (c) $x=0.050$ and (d) $x=0.075$.

Table 1
Bulk density, relative density and porosity of $Mg_{0.9}Mn_{0.1}Tm_xFe_{1.8-x}O_4$ ferrites by SCM.

Composition (x)	Bulk density (g/cm^3)	Relative density (%)	Apparent porosity (%)	Average grain size (μm)
$x=0.0$	4.2604	96.0079	2.5613	2.01
$x=0.025$	4.1103	94.4085	8.5414	1.13
$x=0.050$	3.8654	89.8930	15.5467	0.87
$x=0.075$	3.8207	88.9320	16.4779	0.72

a barrier to the flow of electron, leading to an increase in resistivity of the ferrites [22]. This anticipated consequence in resistivity needs to be confirmed in further observations on the electrical properties.

3.3. Density and porosity measurements

The bulk density and porosity values of $Mg_{0.9}Mn_{0.1}Fe_{1.8-x}Tm_xO_4$ ferrites with different Tm contents are listed in Table 1. It is observed that the bulk density decreases, whilst the porosity increases, with increasing Tm contents. Such a decrease in bulk density and an increase in porosity indicate that densification had been restrained with an increase in Tm contents due to the presence of secondary phases. Consequently, the grain boundary mobility was restrained during sintering. A similar behavior was reported for rare-earth La-doped NiZn ferrites investigated by Sun et al. [23]. The secondary phase in this work, $TmFeO_3$, can be observed in the microstructural images in Fig. 7, and confirmed by EDX analysis.

3.4. Microstructural results

Fig. 7 shows the microstructures by SEM of the sintered ferrites with different amounts of Tm substitutions. The specimen without any substitution (Fig. 7a) shows the presence of a monophasic cubic spinel ferrite phase, whereas the Tm-substituted specimens (Fig. 7b–d) show the presence of a bi-phasic microstructure consisting of a dominant matrix of ferrite grains together with some $TmFeO_3$ secondary phase. The range of grain size presented in Table 1 is 0.7–2 μm. The average grain sizes of the matrix ferrite phase, as well as the $TmFeO_3$ phase, slightly decrease with increasing Tm^{3+} substitutions. It is also suggested that the release of a large amount of gases during the combustion process could contribute to the formation of pores and voids in the specimens [24]. The grain size of the ferrite matrix at $x=0.075$ composition (as observed in Fig. 7d) is relatively lower and it might be due to the inhibition of grain growth due to $TmFeO_3$ phase.

The EDX spectrum (Fig. 8) obtained from the sintered specimens indicates the presence of mainly Tm, Fe and Oxygen along with a small amount of Mg and Mn. This confirmed that the whitish grains are $TmFeO_3$ phase in the microstructure of the sintered Tm substituted Mg–Mn ferrites.

3.5. Magnetic properties

Representative magnetic hysteresis loops for $Mg_{0.9}Mn_{0.1}Tm_x$

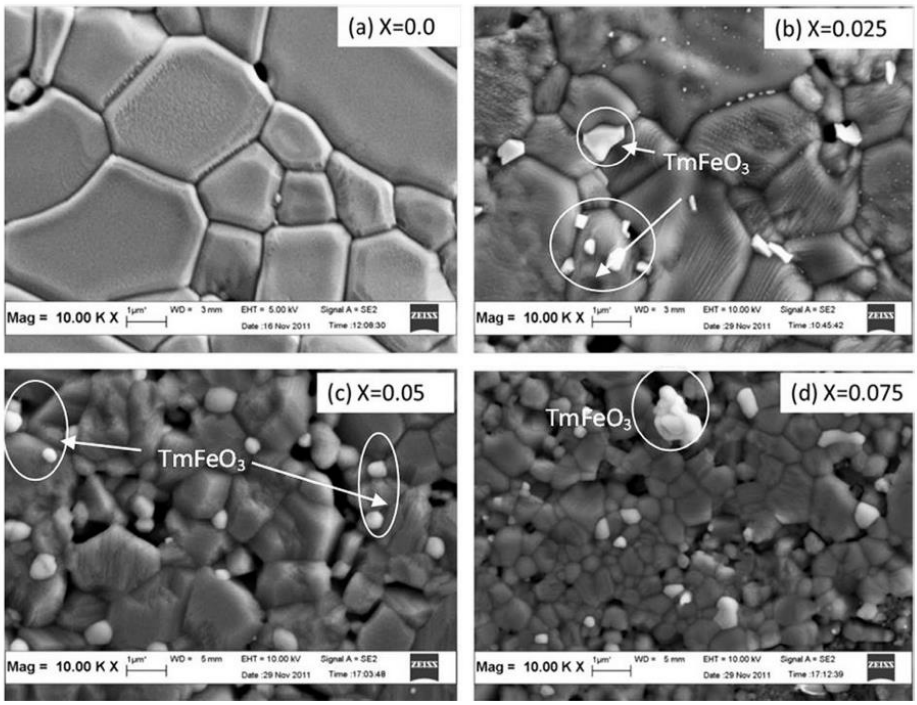

Fig. 7. SEM images of $Mg_{0.9}Mn_{0.1}Tm_xFe_{1.8-x}O_4$ ferrites. (a) $x=0.0$, (b) $x=0.025$, (c) $x=0.050$ and (d) $x=0.075$.

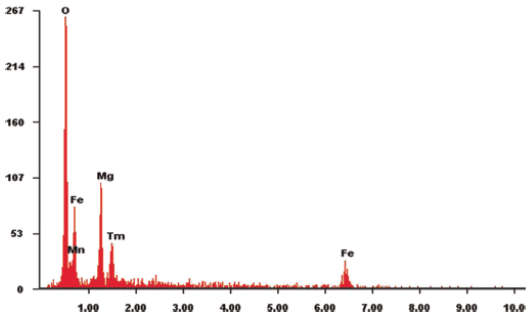

Fig. 8. EDX analysis of $Mg_{0.9}Mn_{0.1}Tm_xFe_{1.8-x}O_4$ ferrite for $x=0.075$ sintered at 1250 °C.

$Fe_{1.8-x}O_4$ ferrites are shown in Fig. 9 which highlight the variations of saturation magnetization and coercivity with varying contents of Tm. It is observed that the magnetization decreases with Tm content. This is correlated to a decrease in density resulting from an increase in the number of pores. It has been found that the presence of pores will hinder the motion of dislocations in solids for the electron spins, and as such, lower the magnetization as observed [25]. Besides, as the grain size decreases, the possibility of domain wall formation becomes less, and hence, the magnetization decreases due to a lesser domain wall movements upon the action of magnetic moments.

Some magnetic properties of the sintered Tm-substituted Mg–Mn ferrites were calculated from the magnetization curves, and

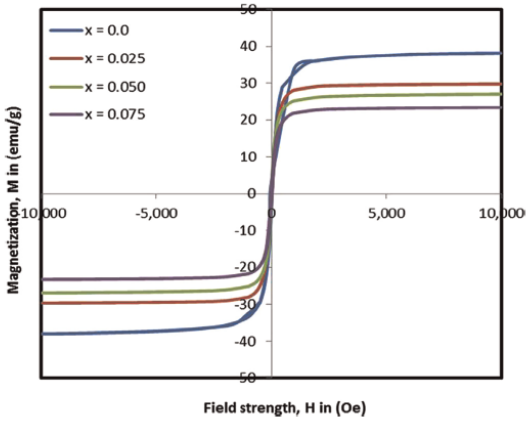

Fig. 9. The magnetization curves of $Mg_{0.9}Mn_{0.1}Tm_xFe_{1.8-x}O_4$ ferrites measured by VSM ± 10 kOe at room temperature.

consequently, M_s, M_r, H_c and n_B are listed in Table 2. It is observed that the coercivity, H_c of the specimens increases with an increase in Tm contents, whilst the saturation magnetization, M_s and the net magnetic moment per unit cell, n_B decrease with increasing Tm contents. The formation of the secondary phase at the grain boundaries may have affected the homogeneous composition and microstructures of the Tm-substituted ferrites. This induces some distortions in the internal grain region, which lead to a larger

Table 2
The values of M_s, M_r, H_c and n_B for $Mg_{0.9}Mn_{0.1}Tm_xFe_{2-x}O_4$ ferrites prepared by SCM with different Tm contents.

Compositions (x)	M_s (emu/g)	M_r (emu/g)	H_c (Oe)	n_B (μB)
$x=0.0$	38.41	0.98	20.25	1.32
$x=0.025$	29.90	2.09	26.53	1.04
$x=0.050$	27.09	2.64	28.00	0.98
$x=0.075$	23.62	4.14	28.38	0.83

internal stress that could possibly affect a decrease in the saturation magnetization [26]. In their work on La-substituted NiCuZn ferrites, Roy et al. [26] had observed a decrease in saturation magnetization at higher concentrations of La in the specimens.

It has been found that the number of grain boundary increases with decreasing number of grain size for a similar volume of sample. In this study, $Mg_{0.9}Mn_{0.1}Tm_xFe_{1.8-x}O_4$ ferrites have smaller grain sizes with increasing amount of Tm contents (Table 1). The region of disordered arrangement of atoms on grain boundaries may possibly fixes and hinders the domain wall motion, resulting in the coercivity of the specimens to increase with Tm contents. The higher value of coercivity observed is attributed to the demagnetization caused by domain rotation, which requires greater energy, rather than the movement of domain walls [27]. The decrease in the magnetic moment per unit cell would also affect the reduction in saturation magnetization of the specimens [28]. Hence, from the results obtained, it is clear that the presence of rare-earth Tm^{3+} ions in amounts of 0.025–0.075 affects significantly and tunes the magnetic properties of the Mg–Mn ferrites.

Table 3 shows the occupation of cations in the tetrahedral A sites and the octahedral B sites as estimated from the observed magnetic moment per unit cell. The values of magnetic moment per unit cell (n_B) are calculated using Eq. (1) and listed in Table 2.

$$n_B = \frac{\text{Molecular weight (Mw)} \times \text{saturation magnetization (Ms)}}{5585} \quad (1)$$

The formula used to propose and calculate the cation distribution of $Mg_{0.9}Mn_{0.1}Tm_xFe_{1.8-x}O_4$ ferrites is

$$\left(Mg_{0.9-y}Mn_zFe_{1-(0.9-y+z)}\right)_A\left[Mg_yMn_{0.1-z}Tm_xFe_{(1.8-x)-(y+0.1-z)}\right]_BO_4 \quad (2)$$

The values of magnetic moments (m) for individual ion for the calculation of cation distributions are $m_{Mg^{2+}} = 0$, $m_{Mn^{2+}} = 5$, $m_{Tm^{3+}} = 7$, and $m_{Fe^{3+}} = 5$, respectively.

In this study, it is observed that, with the substitution of Tm for Fe, the fraction of Tm^{3+} ions predominantly occupy the octahedral-B sites, which are correlated to their preference for larger octahedral site energy. Correspondingly, the fraction of Fe^{3+} ions in octahedral sites decreases linearly. This decrease in Fe^{3+} ions occupying the octahedral sites gives lower magnetization with an increase of Tm content in the Mg–Mn ferrites.

Table 3
Expected cation distribution in $Mg_{0.9}Mn_{0.1}Tm_xFe_{1.8-x}O_4$ ferrites prepared by SCM with different Tm contents.

Compositions (x)	Occupation of cations	
	A site	B site
$x=0.0$	$Mg^{2+}_{0.182}Mn_{0.075}Fe^{3+}_{0.743}$	$Mg^{2+}_{0.718}Mn^{2+}_{0.025}Fe^{3+}_{1.057}$
$x=0.025$	$Mg^{2+}_{0.149}Mn_{0.075}Fe^{3+}_{0.776}$	$Mg^{2+}_{0.751}Mn^{2+}_{0.025}Tm^{3+}_{0.025}Fe^{3+}_{0.999}$
$x=0.050$	$Mg^{2+}_{0.138}Mn_{075}Fe^{3+}_{0.787}$	$Mg^{2+}_{0.762}Mn^{2+}_{0.025}Tm^{3+}_{0.05}Fe^{3+}_{0.963}$
$x=0.075$	$Mg^{2+}_{0.118}Mn_{0.075}Fe^{3+}_{0.807}$	$Mg^{2+}_{0.782}Mn^{2+}_{0.025}Tm^{3+}_{0.075}Fe^{3+}_{0.918}$

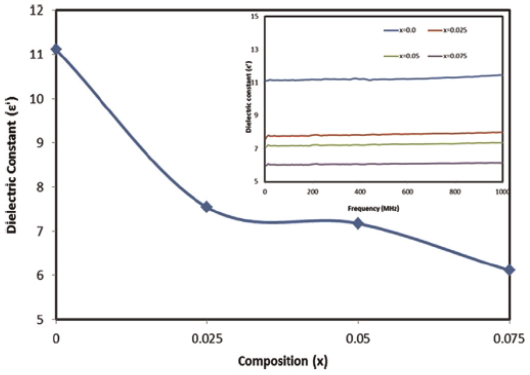

Fig. 10. Variation of dielectric constant with composition for $Mg_{0.9}Mn_{0.1}Tm_xFe_{1.8-x}O_4$ ferrites sintered at 1250 °C.

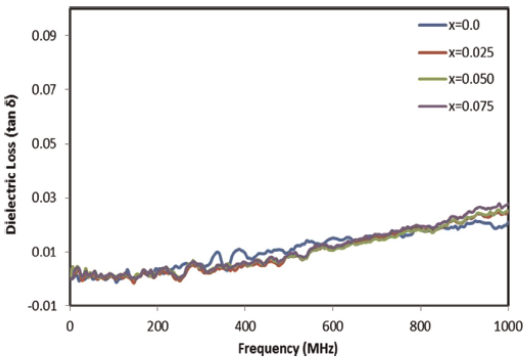

Fig. 11. Variation of loss tangent with frequency for $Mg_{0.9}Mn_{0.1}Tm_xFe_{1.8-x}O_4$ ferrites sintered at 1250 °C.

3.6. Electrical properties

Fig. 10 shows the variation of the dielectric constant (ε') with composition, whilst Fig. 11 shows the dielectric loss tangent (tan δ) of the sintered $Mg_{0.9}Mn_{0.1}Fe_{1.8-x}Tm_xO_4$ ferrite specimens in the frequency range of 1 MHz to 1 GHz. The ε' and tan δ values represent the dielectric properties which refers to the storage capability of electrical energy and the dissipation (or loss) of energy within the medium, respectively. The dielectric constant value was calculated using the following equation [29]:

$$\varepsilon' = \frac{C_p d}{\varepsilon_0 A} \quad (3)$$

where ε_0 is the permittivity of free space, d is the thickness of the specimens, A is the area of cross-section of the pellet specimens and C_p is the measured value of the capacitance of the specimens.

As can be observed from Fig. 10, the specimens sintered at 1250 °C for the different compositions exhibit low dielectric constant and remain nearly constant over the entire frequency range studied as can be observed from the inset in Fig. 10. In general, as the frequency becomes higher (from MHz to GHz), the dielectric constant appears to be almost independent of frequency. This indicates that ferrites with good frequency stability over a wide range from 1 MHz to 1 GHz have been obtained. It has been reported that stoichiometry in composition is an important requirement for obtaining low dielectric constant and low losses

https://www.infona.pl/resource/bwmeta1.element.elsevier-97affe38-f7a1-348f-9f72-1a21e08c4012

http://adsabs.harvard.edu/abs/2015JMMM..385..433L

http://ac.els-cdn.com/S030488531500267X/1-s2.0-S030488531500267X-main.pdf?_tid=7e7fb5a6-4010-11e5-bf97-00000aab0f01&acdnat=1439287709_9028113839000da4d8cdd45cf7a2fe4d